This is an author-created, un-copyedited version of the article G. N. Phung, F.J. Schmückle, R. Doerner, B. Kähne, T. Fritzsch, U. Arz, and W. Heinrich, "Influence of Microwave Probes on Calibrated On-Wafer Measurements," *IEEE Trans. Microw. Theory Techn.*, vol. 67, no.5, pp. 1892-1900, May 2019.

The definitive publisher-authenticated version is available online at:
https://doi.org/10.1109/TMTT.2019.2903400

Influence of Microwave Probes on Calibrated On-Wafer Measurements

Gia Ngoc Phung, Franz Josef Schmückle, Ralf Doerner, *Member, IEEE*, Bernhard Kähne, Thomas Fritzsch, Uwe Arz, *Senior Member, IEEE*, and Wolfgang Heinrich, *Fellow, IEEE*

***Abstract*—On-wafer probing with ground-signal-ground (GSG) probes contributes a variety of side effects, which are related to the measured line type, the carrier material, the layout with the neighboring structures, and the probe. Thus, the size and shape of the probe together with the measured line type and the neighboring circuits influence the quality of the calibrated measured result. This paper presents corresponding results when using the multiline-Thru-Reflect-Line (mTRL) calibration, which is commonly accepted as one of the most accurate calibration algorithms. The paper concentrates on the impact of the probe construction together with neighboring elements, for the most common planar transmission lines, coplanar waveguides (CPW) and thin-film microstrip lines (TFMSL). For the first time, design guidelines with regard to the layout, the measurement environment, and the construction of the probes are given.**

***Index Terms*—Calibration, CPW, electromagnetic field simulation, mTRL, on-wafer probing, probes.**

I. Introduction

As IS well known, on-wafer probing with the common ground-signal-ground (GSG) probes adds parasitic effects, which are related to the device under test (DUT) and the region around, including neighboring structures on the wafer, to the probe and its transition to the pads on the wafer, to the substrate, and to the measurement instrumentation itself.

In [1] the impact of RF probes in monolithic microwave integrated circuits (MMICs) has been investigated. A crosstalk analysis and correction in on-wafer measurements including the RF probes has been presented in [2] at WR-3 (220–325 GHz) band frequencies. In [3] an approach of crosstalk compensation has been presented to improve measurement accuracy. Several publications have already demonstrated the impact of neighboring structures for coplanar waveguides (CPW) on different substrate materials, e.g. GaAs and Al_2O_3 [4], [5]. Similar investigations were presented for the thin-film microstrip line (TFMSL) [6], [7].

The purpose of this paper is to go one step further proposing measures to mitigate the effects caused by non-idealities of the microwave probes. Detailed investigations studying the influence of probe size and geometry, needle length, and the coaxial opening of the probe will be presented for CPW and TFMSL. The investigations performed aim at emulating realistic measurement scenarios using commercially available probes, with a focus on the multiline Thru-Reflect-Line (mTRL) algorithm [8], which is commonly accepted as one of most accurate calibration methods.

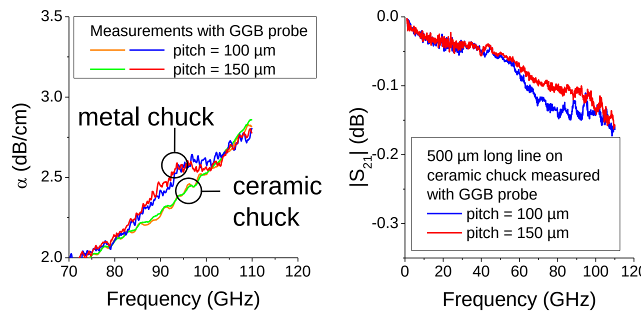

(a) (b)

Fig. 1. Measured results of a set of CPW calibration elements. (a): Attenuation in dB/cm. (b): Transmission coefficient S_{21} of a 500 µm long line measured with probes of different pitch.

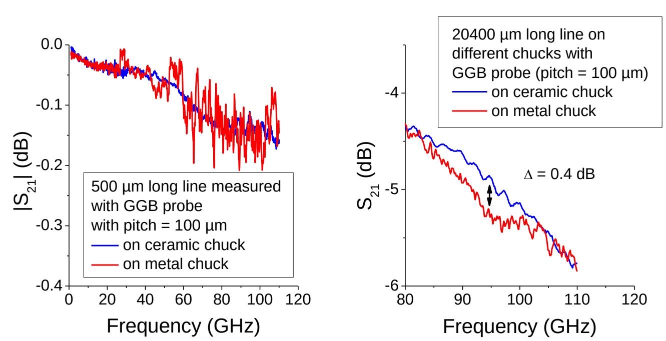

(a) (b)

Fig. 2. Measured results of a set of CPW calibration elements on different chuck materials. (a): Transmission coefficient S_{21} of a 500 µm long line. (b): Transmission coefficient S_{21} of a 20400 µm long line (zoomed).

In general, the calibration procedure is based on three steps, (i) measuring the standards, (ii) calculating the error matrix, and (iii) applying the error matrix to obtain the true performance of the DUT. The mTRL calibration is based on the assumption of single-mode propagation. So, this procedure

Manuscript received September 30, 2018; revised November 23, 2018. This work was supported by the European Metrology Programme for Innovation and Research (EMPIR), Project 14IND02, and partly funded by the German BMBF InPro3D program, Project NaLoSysPro.

G. N. Phung, F. J. Schmückle, R. Doerner, B. Kähne and W. Heinrich are with the Ferdinand-Braun-Institut für Höchstfrequenztechnik (FBH), 12489 Berlin, Germany.

T. Fritzsch is with the Fraunhofer Institut für Zuverlässigkeit und Mikrointegration (IZM), 13355 Berlin, Germany.

U. Arz is with the Physikalisch-Technische Bundesanstalt (PTB), 38116 Braunschweig, Germany.

is only valid as long as there are no perturbations by additional modes excited due to the measurement boundary conditions and if there is no coupling from the probe to neighboring structures.

Figs. 1 and 2 illustrate the case for the propagation constants extracted from a CPW calibration set built on an alumina substrate [5], measured with probes from the same manufacturer but with different probe pitches and on different chucks. The measurements reveal several irregularities. Obviously, the selection of chuck material can lead to divergent behavior in the measurement results, as can be observed in the attenuation extracted from a CPW calibration set (Fig. 1(a)) and in the ripples in the transmission coefficient of a 500 µm long CPW (Fig. 2(a)). Fig. 1(b) refers to the same DUT measured with probes from the same manufacturer, but with different probe pitches also a divergent behavior is revealed. With this motivation, this paper aims to clarify the reasons which are responsible for peculiarities in the measurements.

The first part of this paper presents detailed investigations on the impact of the probe construction, which form the basis for the design guidelines. The CPW case is treated and the investigations are limited to the frequency range up to 70 GHz, in order to focus on the influence of the probes and hence to exclude radiation and higher-order mode propagation. The second part of the paper then adds measurement data for the case of the TFMSL, in order to verify the developed design guidelines. In the latter case, we cover the full W-band since the TFMSL is much less affected by radiation and parasitic modes.

II. Investigation of Coplanar Waveguides

Our aim is to identify the perturbing effects which appear in the calibrated results, due to the non-ideal properties of probes and the environment. The way the wafer or chip with the DUT is measured plays an important role in this regard. Therefore, we assume three different lower boundary conditions in our investigations:

1. ceramic sub-substrate (chuck), $\varepsilon_r = 6$, denoted as L1
2. metal backside (chuck), denoted as L2
3. half-infinite extension, denoted as L3

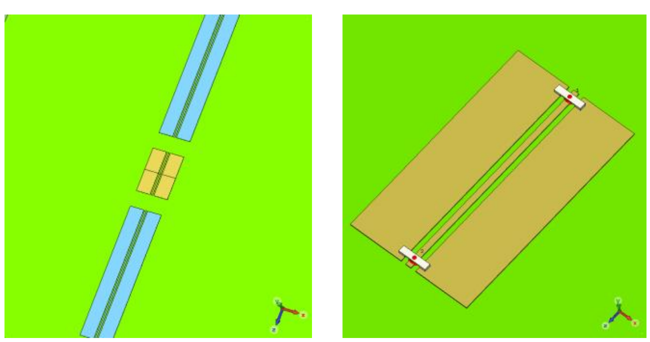

(a) (b)

Fig. 3. (a): Thru line 550 µm; neighboring lines (blue) are not present in the simulation but only maintain consistent discretization for all investigations. (b): Bridge model used as a reference for comparison.

The structure under investigation is a common CPW with a signal width w = 18 µm, a gap of g = 16 µm, a ground (GND) metal width of m = 175 µm and a metal thickness of t = 3 µm on GaAs substrate (ε_r = 12.9). The investigated dimensions of the CPW structures are used to demonstrate the effects and might not be compatible with all commercially available probes. All results presented here, both simulated and measured ones, have been processed through a mTRL calibration process. Each calibration set consists of a short (access line length 800 µm, total length 3700 µm), an open (lengths as in short), a thru (550 µm, Fig. 3) and lines of lengths 667, 900, 1600, 2685, 3700, 7115 and 10000 µm. The first set of investigations concern the measured CPW lines as DUT only, without any neighboring structures. The idea behind this is to determine the effects without any probe coupling to neighboring structures. In the second step, the influence of neighboring elements varying their shape and position is introduced successively. In both sets different types of probes are applied. The probe geometries are generic but emulate realistic commercial probes. Some details are exaggerated on purpose, in order to emphasize the respective electromagnetic effects.

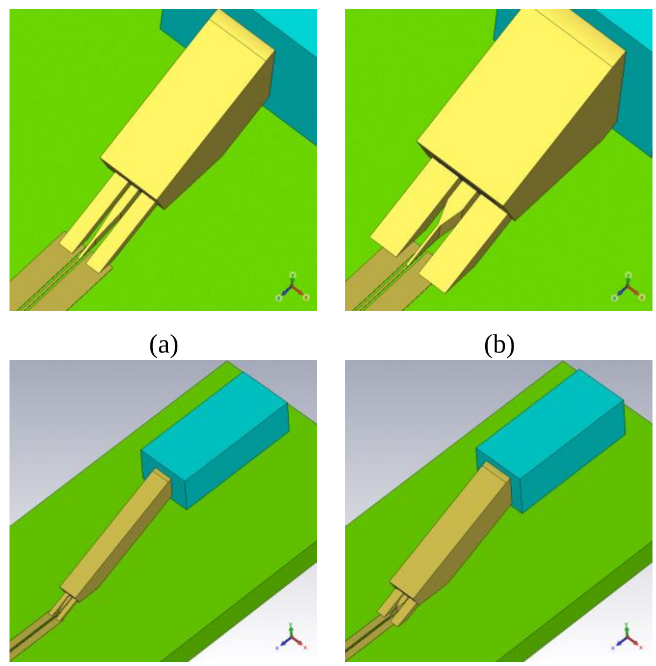

(a) (b)

(c) (d)

Fig. 4. Basic probe geometry. (a): Probe 1.1 with slant (1000 µm). (b): Probe 2.1 (scaled version of probe 1.1, lateral dimensions doubled). (c): Probe 1.2 with longer slant (3000 µm). (d): Probe 2.2 (scaled version of probe 1.2, lateral dimensions doubled).

The basic probe configuration is shown in Fig. 4. For the basic probe version, simple needles are used, formed in a shape so that they fit to the signal width of the CPW. The rectangular probe is slanted and transitions into a horizontal coaxial line in order to allow waveguide ports (necessary in time domain solver of Microwave Studio from Computer Simulation Technology (CST)). The coaxial line is assumed to have rectangular cross-section, in order to save discretization cells, and terminates at the waveguide port. The absorber (ε_r = 17.3, and tanδ = 0.19 at f = 50 GHz) is extended beyond this point to suppress unwanted fields in the reverse direction. The inner signal line of the coaxial probe also features a square cross section, with a diameter which forms a 50-Ω system. The angle of the probe is 25°, if not specified differently. This angle is important for parasitic modes bound between the GND of the probe and the metalizations and dielectric below the probe.

The resulting types of probes are depicted in Fig. 4. Two sizes are used with two different lengths (1 and 3 mm) of slants. In the course of the paper some modifications of these probes will be studied as well, varying the absorber size and probe angle. But the four types of probes shown in Fig. 4 serve as a basis throughout the paper.

All data presented refer to calibrated results, i.e., also the simulation data is obtained by first simulating the full calibration set and performing the mTRL calibration on this data. Thus, the procedure is identical to that used for the measurements, which is decisive in order to ensure consistency between measured and simulated data.

III. Bridge Excitation

As a reference the probes can be compared to simulations, where a simplified bridge model (see Fig. 3(b)) is used, which represents the port connection with least parasitics, i.e., the ideal probe, as has been verified for CPW structures in various cases (see, e.g. [9] and [10]).

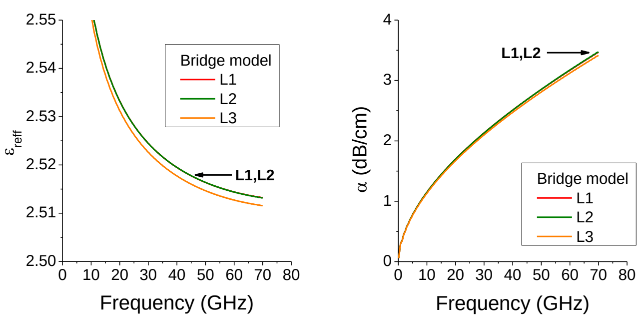

(a) (b)

Fig. 5 (a): Effective permittivity. (b): Attenuation in dB/cm for different boundary conditions.

Fig. 5 presents the propagation constants extracted from calibration when using this bridge excitation. As can be seen, the curve behavior looks completely clean and values for the three different boundary conditions are almost identical, as it should be in the ideal case.

IV. Simulation of Single DUT with Different Probe Types

The starting point of our investigation is the simulation of the DUT without any perturbations due to neighboring structures. Only the DUT is left, which is contacted using the different probe types shown in Fig. 4.

Fig. 6 reveals that in the case of the ceramic chuck L1 the propagation constants are consistent for all probe types. The curve behavior is comparable and only small deviations can be detected.

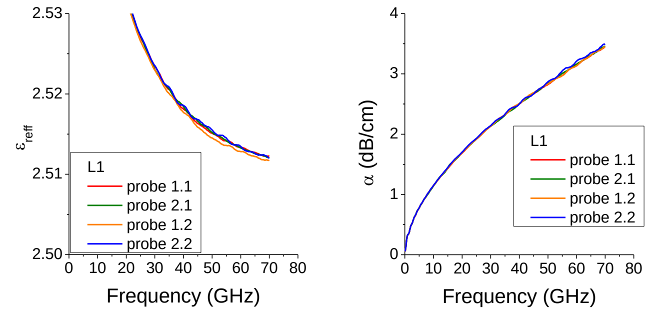

(a) (b)

Fig. 6. Effective permittivity (a) and attenuation (b) when using the ceramic chuck (L1). For probe types refer to Fig. 4.

Figs. 7–9 indicate, however, that the consistency of the extracted propagation constants does not mean that the results for a DUT are consistent either. Simulating the CPW line 3 with a length of 1600 µm reveals different curve behaviors compared to the bridge model for the different boundary conditions. This indicates that even for a configuration without neighboring line structures, the mTRL calibration cannot completely compensate the probe influence. However, the deviations remain below 1%. The question now is whether and how these relatively small deviations change when neighboring structures are added.

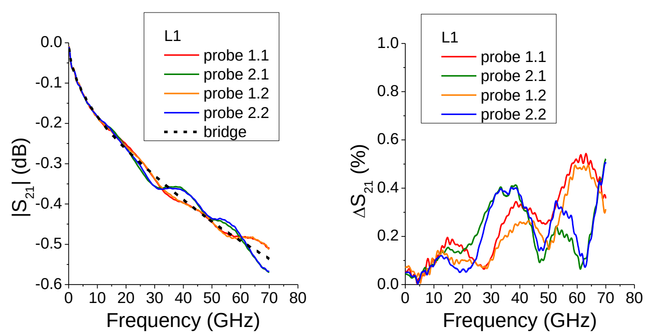

(a) (b)

Fig. 7. Calibrated results of line 3 (1600 µm) on ceramic chuck (L1). (a): Transmission S_{21}. (b): Deviation ΔS_{21} to bridge model.

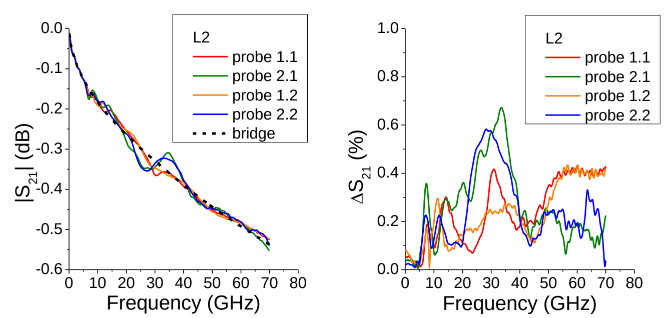

(a) (b)

Fig. 8. Calibrated results of line 3 (1600 µm) on metal chuck (L2). (a): Transmission S_{21}. (b): Deviation ΔS_{21} to bridge model.

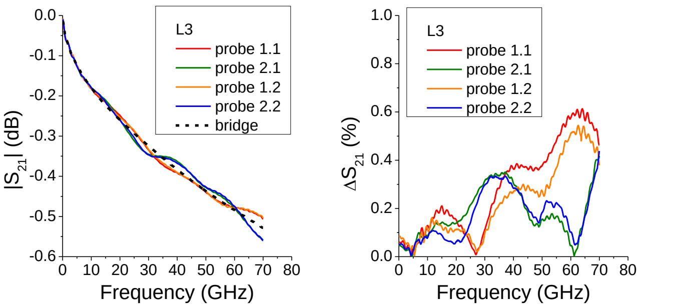

(a) (b)

Fig. 9. Calibrated result of line 3 (1600 µm) for infinite substrate (L3). (a): Transmission S_{21}. (b): Deviation ΔS_{21} to bridge model.

V. Impact of Neighboring Structures

A. Impact of In-line Neighbors

In practical applications, the structures are placed on the wafer in a dense way with small spacing between the elements and to the wafer edge, in order to save precious wafer area. In many cases, the structures are placed in the same grid, which means the inputs/outputs of the DUT are in line with other neighboring structures on the wafer. Therefore, it is important to understand the influence of in-line neighbors on the DUT results. In the following, this is investigated by varying first the distance between the in-line neighbor and the measured DUT and then the shape of the in-line neighbor. The term "in-line" means here that the neighboring line structure is oriented in the same way and the lateral offset between the two centers is zero.

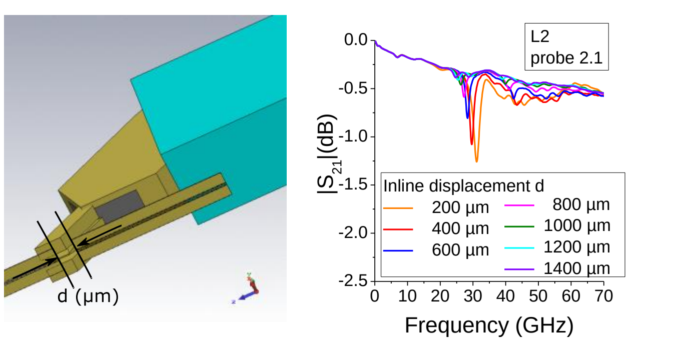

(a) (b)

Fig. 10. (a): Line 3 as DUT, contacted with probe 2.1, with an in-line CPW line of length 1667 µm at an initial distance d = 200 µm (with the substrate hidden). (b): Transmission coefficient with varying distance to the in-line neighbor, d = 200…1400 µm, for metal chuck (L2).

Fig. 10(a) illustrates this configuration when contacting a DUT (line 3) with probe 2.1 and having an in-line CPW underneath the probe.

The length l = 1667 µm of the neighboring CPW is chosen to yield a resonance behavior around 30 GHz. Then, the in-line neighbor is shifted in in-line direction, further away from the DUT, covering a distance between d = 200 µm and 1400 µm (Fig. 10(b)). As expected, when reducing the distance of the neighboring structure an artifact in the transmission coefficient appears (Fig. 11) as dip around 30 GHz, the resonance frequency of the neighboring line. Another observation is that the lower boundary condition determines the strength of the dip. The case of a metal backside (L2) represents the worst case whereas the other cases with ceramic chuck and infinite substrate (L1, L3) reveal similar results. It is also clearly visible that the probes with the larger dimensions (2.1 and 2.2) always yield larger deviations, because the probe dimension determines how strongly the probe couples to the structures on the wafer.

B. Differently Shaped In-line Neighbors

In order to prove that the CPW mode of the neighboring structure is responsible for the dip behavior, we studied the case when the neighboring CPW structure is replaced by a metal patch and varied also the dimensions of this patch. Fig. 12 presents the results.

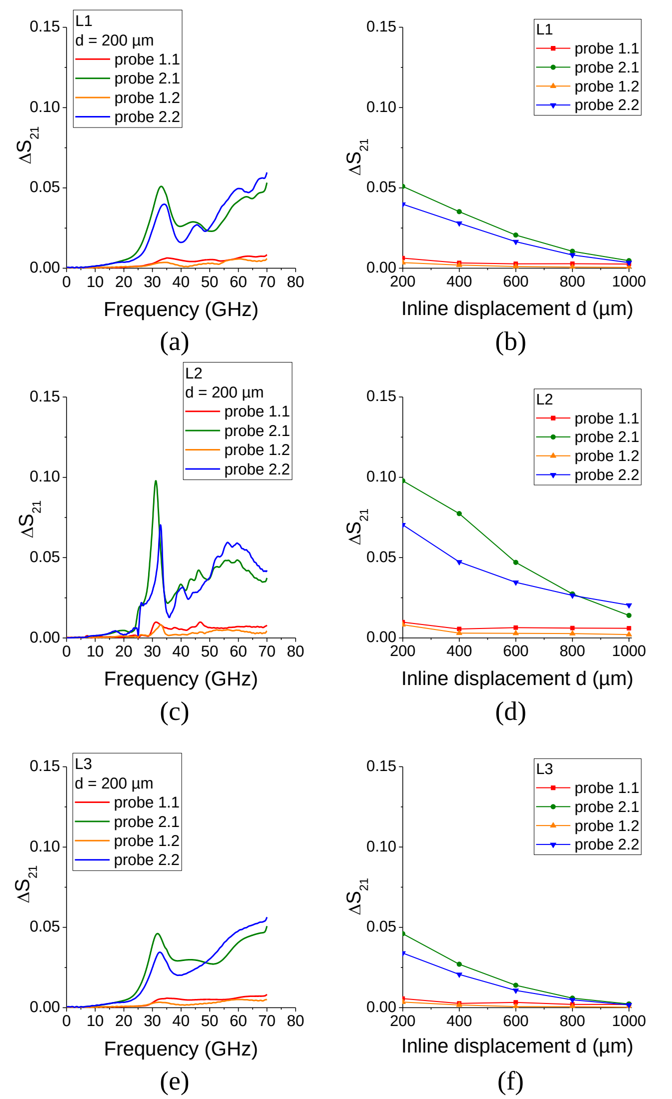

Fig. 11. Transmission S_{21}: Relative difference to the case with distance d = 1400 µm. (a), (c), (e) Deviations for d = 200 µm as a function of frequency for the chuck arrangements L1…L3. (b), (d), (f) Maximum deviation up to 70 GHz as a function of in-line distance d for the chuck arrangements L1…L3.

The standard case is the CPW in-line neighbor investigated also in the previous subsection. Two other cases are added, the metal patch with larger width (denoted as wide) and a patch of shorter length but larger width (ext). The distance to the DUT is kept constant at 200 µm. One finds that only the standard case with a CPW resonator reveals the dip behavior and none of the other structures show this behavior in the investigated frequency range. This proves clearly that the excitation of the resonance in the in-line neighbor is responsible for the dip behavior. Different shapes of the in-line neighbors lead to deviations in the S parameters compared to the bridge model, but to a much smaller extent.

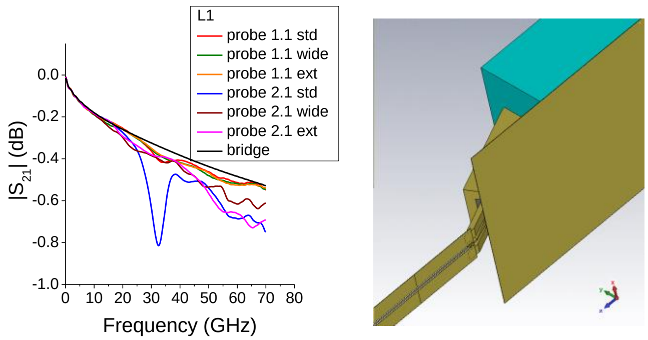

(a) (b)

Fig. 12. (a): Influence of in-line neighbors of different shape on the calibrated result of line 3, in-line CPW (std), patch with larger width (wide), patch shortened and extended sideways (ext), and case with bridge excitation instead of probes. (b): In-line CPW neighbor replaced by a metal patch with larger width (wide) (substrate hidden).

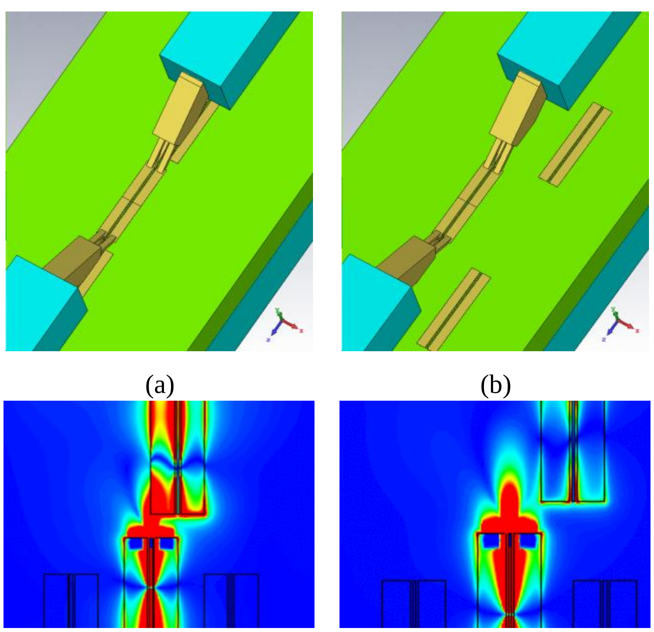

(a) (b)

(c) (d)

Fig. 13. Top: DUT line 3 measurement with probe 1.1 and the in-line CPW neighbor offset from the center line of the DUT. The initial distance to the DUT in the symmetrical case is again 200 µm. (a): Offset s = 100 µm; (b): Offset s = 1000 µm. Bottom: Field plots illustrating the coupling to the in-line neighbor for s = 200 µm (c) and s = 400 µm (d).

C. Sideways Shifted In-line CPW

In the previous investigations, the in-line neighbor is positioned directly underneath the probe. Hence, the question is what happens if the in-line neighbor is shifted sideways. This is investigated in the following (see Fig. 13).

The field plots in Fig. 13 suggest that when increasing the offset first the coupling from the probe to the CPW mode on the neighboring structure decreases but instead now the slot-line mode is excited there (see Fig. 13(c), for an offset of 200 µm). Only when further increasing the offset, moving the structure outside the probe shadow, the excitation is reduced in general (see Fig. 13(d)).

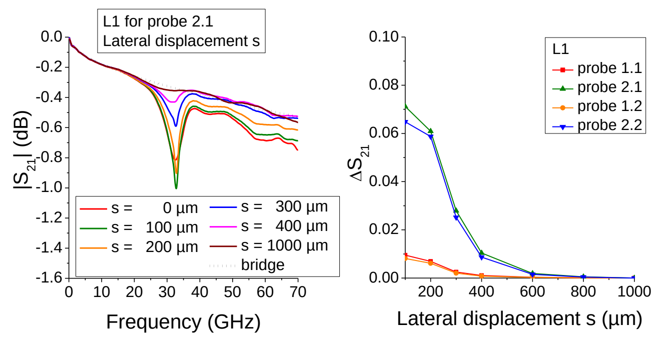

(a) (b)

Fig. 14. Transmission S_{21} of line 3 for probe 2.1 on ceramic chuck (L1) (a) and lateral offsets s = 0…1000 µm. Maximum deviation up to 70 GHz as a function of lateral offset for different probes (b).

Fig. 14(a) shows the transmission for the lateral offsets between s = 0 µm and s = 1000 µm for probe 2.1. Fig. 14(b) reveals that larger probe dimensions (probe 2.1 and probe 2.2) show higher deviations. With increasing lateral offsets, the deviations decrease for the investigated probes. These results prove that with increasing offset the dip behavior is reduced indeed. As long as the in-line neighbor is located outside the probe shadow, the influence is negligible.

D. Modifying the Probes

So far, we have used standard probe dimensions which are typical and comparable to commercial probes. In this section, we discuss special modifications of the probes, varying the size of the absorber and the probe angle (Figs. 15 and 16).

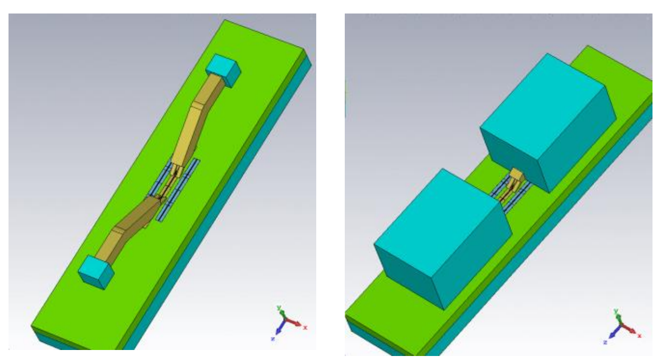

(a) (b)

Fig. 15. Different absorber sizes around the probes. (a): shortened absorber denoted as "less absorber". (b): extended absorber size denoted as "thick absorber".

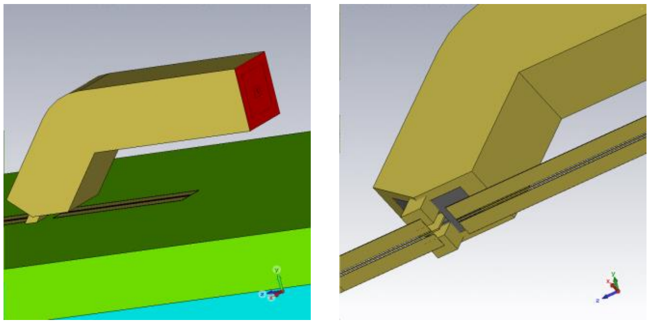

(a) (b)

Fig. 16. (a) Modified probe 2.1 with an angle of 50° instead of 25° (b) with the substrate hidden.

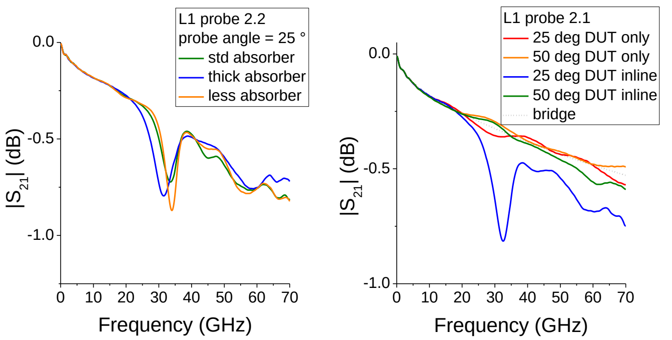

(a) (b)

Fig. 17. Impact of absorber sizes for probe 2.2 and 25° probe angle (a) and for probe 2.1 and different probe angles with and without in-line neighbor (b). Bridge excitation is shown as reference.

Three different cases of absorber size are investigated using standard absorber size, a shortened and a thick absorber version. Fig. 17(a) reveals that independently of the absorber size the influence of the dip behavior is still present. This is because the common absorber material is not efficient enough to suppress the coupling in this case (while it may be helpful to suppress other unwanted modes on the outer side of the coaxial structure).

On the other hand, the probe angle is a parameter which is essential for the dip behavior. Fig. 17(b) shows that applying a larger probe angle (50°) the dip behavior almost disappears, because the coupling effects are reduced. However, implementing a steeper angle may have practical limitations in probe mechanics and would also prevent using a top-down microscope assisting in positioning the probes.

VI. Design Guidelines and Verification

Summarizing the above results, one can state that coupling between the probes and other structures in the vicinity is the main problem. Resonances of the neighboring structures show up as dips or peaks in the frequency dependence of the DUT S parameters after calibration. The strength of these effects is governed by the dimensions of the probes. Relevant is the effective area on the lower side of the probe which we describe as "probe shadow" (see Fig. 18). This is determined mainly by the size and length of the probe needles and the angle at which they touch down to the wafer. Also, the choice of the chuck material influences the strength of the dip behavior. Using a metal chuck represents the worst case. A ceramic chuck or infinite chuck yield better results, at a similar level.

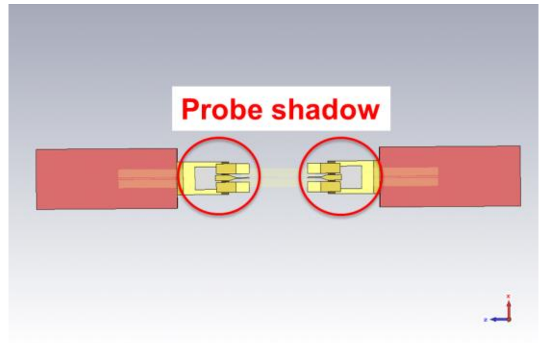

Fig. 18. Defining the critical area below the probes.

The consequence on the circuit design side, i.e., for the layout, is as follows: One should keep the probe shadow (see Fig. 18) free to avoid probe coupling to neighboring structures.

A. Verification for the CPW Case

The first step in validating the design guidelines was to characterize a GaAs-wafer with CPW lines that has been used in [4] already. Fig. 19 presents the layout of this wafer and the two structures studied in the following.

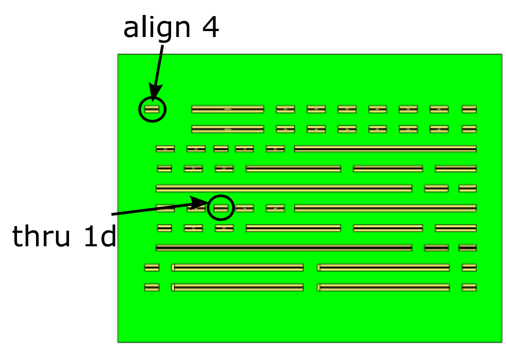

Fig. 19. The layout of the GaAs wafer [4] and the DUTs under investigation.

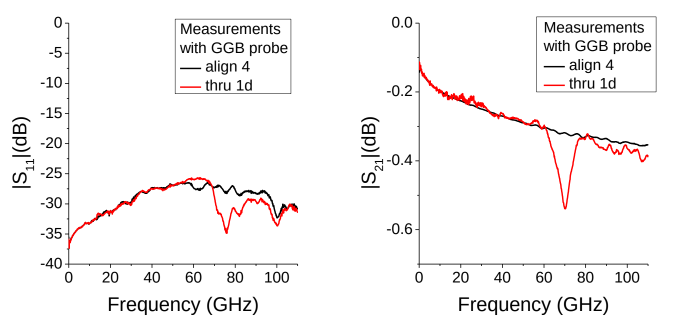

(a) (b)

Fig. 20. Magnitude of S_{11} (a) and S_{21} (b) measurements for the two DUTs in Fig. 19.

The CPWs have a signal width of 25 µm, 15 µm gap, and a metal thickness of 0.5 µm. The length of the mTRL calibration remains the same as in Sec. II. The measurements are performed on a ceramic chuck (ε_r = 6). The probe used for the measurement has a pitch of 100 µm. The investigated DUTs are marked in Fig. 19. DUT "align 4" is an element which is placed far away from other neighboring structures with an in-line distance of 1275 µm. This ensures that the critical area below the probe shadow is free of structures. On the other hand, "thru 1d" is identical in layout, but is placed closely to other neighboring structures with different in-line distances on each side of 300 and 350 µm.

The corresponding measurements for the two structures are plotted in Fig. 20. The results reveal a dip behavior in S_{21} for "thru 1d" while for "align 4" a smooth curve is observed. As can be seen from Fig. 19, "align 4" is placed apart from other structures, following the above design guidelines, while "thru 1d" is not. Thus, the curves in Fig. 20 prove validity of the guidelines for this case.

However, further investigations revealed that it is not easy to verify the design guidelines on probe coupling for the CPW case in a more general way, because it is difficult to differentiate the parasitic effects due to substrate modes from probe coupling [4].

Hence, the thin-film microstrip is used for this purpose in the following. In contrast to the CPW case, the TFMSL environment excludes substrate modes and thus forms the ideal vehicle to study coupling between the probe and the surrounding structures by fringing fields.

B. Verification using Thin-Film Microstrip

The TFMSL process used here comprises a thin-film multilayer stack which is realized on top of a 700 µm thick Borofloat substrate. The ground layer is buried in 16 µm thick benzocyclobutene (BCB) (ε_r = 2.65) with a layer stack, the signal strip metallization level (with a thickness t = 11.1 µm) is located on top of the BCB and an intermediate metal layer level can be added. This process was developed at Fraunhofer IZM as motherboard for microwave modules and is suited as an example for other thin-film wafer topologies as well.

Fig. 21 shows the layout of the calibration set and the test structures used for verification. The calibration set consists of calibration line elements comprising 4 TFMSL lines (signal width w = 37 µm) of different lengths (l = 900, 1800, 2700 and 5400 µm without pads), as well as an open and a short structure as reflect standards. The pad includes a CPW-to-MS transition for probing. Loads cannot be designed because resistors were not available on this specific wafer run. An additional load structure would enable the transformation of the reference impedance [11], e.g. to 50 Ω. The calibration structures are placed on the wafer with large spacing to the neighboring structures to obtain clean values for calibration. This is obtained without sacrificing a lot of area since the coupling of adjacent TFMSL structures is governed by the ratio of lateral distance to substrate thickness: Since the respective BCB thickness is only 16 µm, lateral distances in the 700 µm range already yield ratios of over 40.

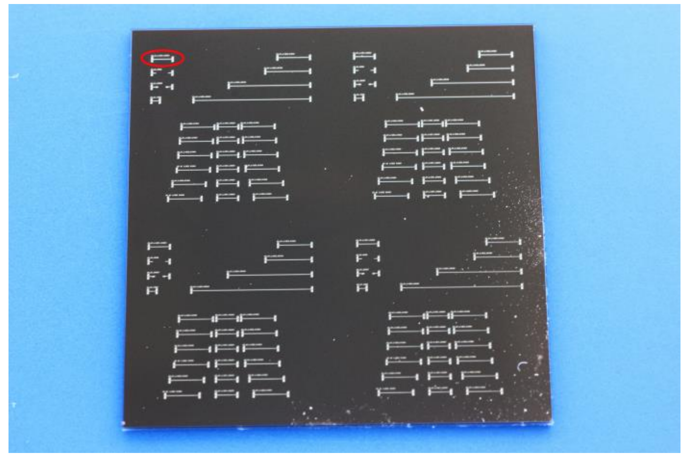

Fig. 21. TFMSL wafer designed and manufactured for verification. Marked DUT as reference structure with large distances to neighboring structures.

The test structures are placed on a test field shown in Fig. 22(b). Here, the same structure with identical layout is placed on the test field with varying in-line distance. This emulates the previous investigations.

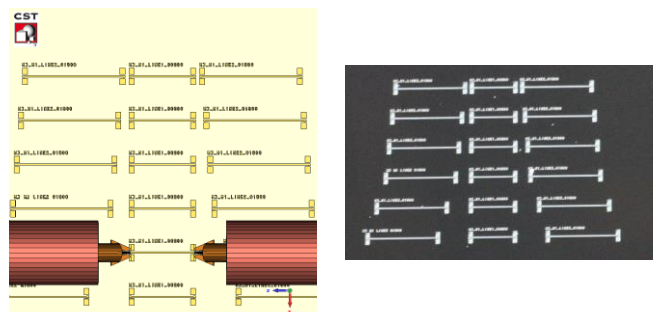

(a) (b)

Fig. 22. Zoomed version of the wafer with probe (a) in Microwave Studio (CST) illustrating the case with an in-line distance of 700 µm, where the in-line neighbor is outside the probe shadow. Wafer layout (b) used for verification.

Figs. 23 and 24 show simulated and measured data for the same structures. Good agreement is found. Overall, there is a slight shift in frequency, but this can be traced back to the uncertainty in material properties and a certain lack of knowledge of details of the probe geometries. Both figures confirm the statement that, as long as the in-line neighbor is outside the probe shadow (see Fig. 22(a), where the in-line distance is about 700 µm), the dip behavior disappears.

Complementing the results of Figs. 23 and 24, we performed additional measurements with probes from another vendor (Cascade Microtech, now Form Factor), which are plotted in Fig. 25. It can be seen that they show a different behavior at the peak, due to the different probe geometries. However, the above recommendation to keep the probe shadow free of structures holds also for another probe type.

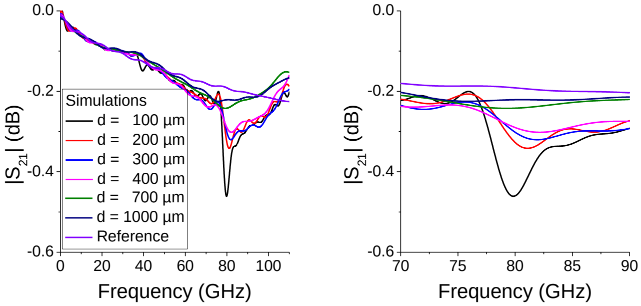

(a) (b)

Fig. 23. (a) Calibrated simulation results for varying in-line distance from 100 to 1000 µm. (b): Zoomed area where the peak or resonance behavior can be seen.

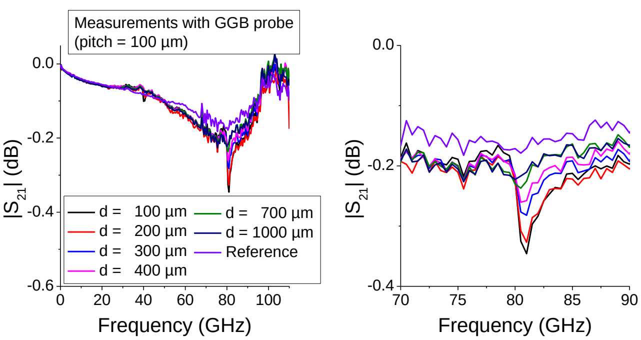

(a) (b)

Fig. 24. Measurement data corresponding to Fig. 23.

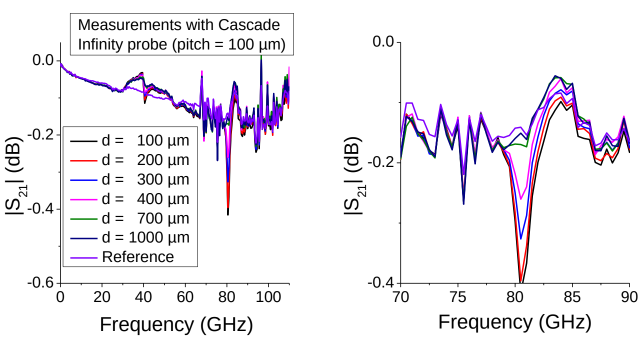

(a) (b)

Fig. 25. Measurements of Fig. 24 with a different commercial probe.

VII. Conclusion

The results presented clarify in which way realistic probe geometries influence the accuracy of TRL-calibrated *S* parameter measurements. In conclusion, the design guideline for the wafer layout is to keep the region of the probe shadow free of structures. On the probe side, this means: One should keep this shadow to a minimum, i.e., keep the needles short and use a touch-down angle as steep as possible. The absorber material along the coaxial feeder, on the other hand, has not much influence for this type of coupling. These guidelines apply to CPW and TFMSL in the same way.

Acknowledgment

The authors would like to thank S. Schulz, J. Schmidt and T. Probst for performing measurements.

References

[1] D. Müller *et al.*, "Electromagnetic Field Simulation of MMIC including RF Probe Tips," in *Proc. 47th European Microwave Conf. (EuMC)*, Nuremberg, Germany, Oct. 2017, pp. 900–903.

[2] D. Müller, F. Boes, A. Tessmann, A. Leuther, T. Zwick, I. Kallfass, "Crosstalk Analysis and Correction in On-Wafer Measurements at WR-3 Band Frequencies," in *2018 German Microwave Conf. (GeMiC)*, Freiburg, Germany, Mar. 2018, pp. 160–163.

[3] D. F. Williams, F. J. Schmückle, R. Doerner, G. N. Phung, U. Arz, W. Heinrich, "Crosstalk Corrections for Coplanar –Waveguide Scattering-Parameter Calibrations," *IEEE Trans. Microw. Theory Tech.*, vol. 62, no. 8, pp. 1748-1761, Aug. 2014.

[4] F. J. Schmückle, T. Probst, U. Arz, G. N. Phung, R. Doerner, W. Heinrich, "Mutual Interference in Calibration Line Configurations," in *89th ARFTG Microwave Measurement Conf. Dig.*, Honolulu, HI, USA, Jun. 2017.

[5] G. N. Phung, F. J. Schmückle, R. Doerner, W. Heinrich, T. Probst, U. Arz, "Effects degrading accuracy of CPW mTRL calibration at W Band," in *2018 IEEE MTT-S Int. Microwave Symp. Dig.*, Jun. 2018, pp. 1296–1299.

[6] G. N. Phung, F. J. Schmückle, W. Heinrich, "Parasitic Effects and Measurement Uncertainties in Multi-Layer Thinfilm Structures," in *Proc. 43rd European Microwave Conf. (EuMC)*, Nuremberg, Germany, Oct. 2013, pp. 318–321.

[7] G. N. Phung, F. J. Schmückle, R. Doerner, T. Fritzsch, W. Heinrich, "Impact of Parasitic Coupling on Multiline TRL Calibration," in *Proc. 47th European Microwave Conf. (EuMC)*, Nuremberg, Germany, Oct. 2017, pp. 835–838.

[8] R. B. Marks, "A Multiline Method of Network Analyzer Calibration," *IEEE Trans. Microw. Theory Techn.*, vol. 39, no. 7, pp. 1205–1215, Jul. 1991.

[9] T. K. Johansen, C. Jiang, D. Hadziabdic, V. Krozer, "EM Simulation Accuracy Enhancement for Broadband Modeling of On-Wafer Passive Components," in *Proc. 37th European Microwave Conf. (EuMC)*, Munich, Germany, Oct. 2007, pp. 1245–1248.

[10] U. Arz, M. Rohland, K. Kuhlmann, S. Büttgenbach," Wideband Electromagnetic Modeling of Coplanar Waveguides Fabricated in Membrane Technology," in *15th IEEE Workshop on Signal Propagation on Interconnects (SPI)*, May 2011, pp. 129–130.

[11] D. F. Williams and R. B. Marks, "Transmission line capacitance measurement," *IEEE Microw. Guided Wave Lett.*, vol. 1, no. 9, pp. 243–245, Sep. 1991.